Géotechnique Letters

Analysis of the added mass term in soil bearing capacity problems

--Manuscript Draft--

Manuscript Number:	GLETT-D-20-00097R2
Full Title:	Analysis of the added mass term in soil bearing capacity problems
Article Type:	Paper
Corresponding Author:	Katherine Kwa University of Southampton Civil and Environmental Engineering Southampton, UNITED KINGDOM
Corresponding Author Secondary Information:	
Corresponding Author's Institution:	University of Southampton Civil and Environmental Engineering
Corresponding Author's Secondary Institution:	
First Author:	Katherine Kwa
First Author Secondary Information:	
Order of Authors:	Katherine Kwa
	Gabriel Weymouth
	David White
	Chris Martin
Order of Authors Secondary Information:	
Abstract:	This technical note presents a simplified method for quantifying the added mass of the soil that is mobilised as part of the failure mechanism around a foundation during rapid loading, and the resulting additional soil resistance. This note focuses on the solutions for an embedded plate anchor, which is a potential foundation system for offshore floating facilities. In current practice, only the shear strength of the soil surrounding the foundation is considered in calculations of the ultimate bearing capacity. However, the solutions presented in this technical note show that the added mass of the soil involved in the failure mechanism around the foundation can result in a significant increase in ultimate bearing capacity during extreme dynamic wave loading events. These lead to snatch loads transmitted to the anchoring and mooring system, which are high but brief. The technical note provides a general approach applicable to all foundation types, and illustrates the effect of the added mass term and the additional capacity for an embedded plate anchor with typical input conditions.

Analysis of the added mass term in soil bearing capacity problems

Kwa, K.A.[*], Weymouth, G.D. [*], White, D.J. [*] & Martin, C.[#]
[*]Civil and Maritime Environmental Engineering, The University of Southampton, United Kingdom
[#]Civil Engineering, The University of Oxford, United Kingdom

---

We thank the Assessor and Reviewer for their time in reviewing our paper, for the positive responses and for their helpful comments. We have attached the files required for the final submission of this manuscript. Please let me know if anything further is required and we look forward to receiving the typeset proofs.

Kind Regards,
Katherine.

Analysis of the added mass term in soil bearing capacity problems

K.A. Kwa, G.D. Weymouth, D. J. White, C.M. Martin,

Katherine A. Kwa, BEng, PhD
University of Southampton, Southampton, SO17 1BJ, UK
k.a.kwa@soton.ac.uk

Gabriel D. Weymouth, ScD, MSc, BSc
University of Southampton, Southampton, SO17 1BJ, UK
g.d.weymouth@soton.ac.uk

David J. White, BA, MA, MEng, PhD (Cantab), FREng, FICE, FTSE, FRINA, FIEAust
University of Southampton, Southampton, SO17 1BJ, UK
david.white@soton.ac.uk

Chris Martin, BE, DPhil
University of Oxford, Department of Engineering Science, Parks Road, Oxford OX1 3PJ, UK
chris.martin@eng.ox.ac.uk

Number of words (excluding abstract, acknowledgements, references, tables and figure captions): 2002

Number of tables: 3

Number of figures: 5

Analysis of the added mass term in soil bearing capacity problems

ABSTRACT

This technical note presents a simplified method for quantifying the added mass of the soil that is mobilised as part of the failure mechanism around a foundation during rapid loading, and the resulting additional soil resistance. This note focuses on the solutions for an embedded plate anchor, which is a potential foundation system for offshore floating facilities. In current practice, only the shear strength of the soil surrounding the foundation is considered in calculations of the ultimate bearing capacity. However, the solutions presented in this technical note show that the added mass of the soil involved in the failure mechanism around the foundation can result in a significant increase in ultimate bearing capacity during extreme dynamic wave loading events. These lead to snatch loads transmitted to the anchoring and mooring system, which are high but brief. The technical note provides a general approach applicable to all foundation types, and illustrates the effect of the added mass term and the additional capacity for an embedded plate anchor with typical input conditions.

KEYWORDS

Analysis, added mass, ultimate bearing capacity, embedded plate anchors, foundations

Manuscript submitted for publication on 23 May 2020

LIST OF SYMBOLS

A area

a acceleration

α offset value

B plate width

E kinetic energy

F total resistance force

F_{AM} added mass resistance force

F_{load} design wave load

F_{min} steady static component of mooring load

F_{max} peak load

F_{su} static geotechnical capacity

$\tilde{\kappa}$ local kinetic energy of the flow per unit mass

m_{AM} added mass

m_{plate} mass of the plate

N_{AM} dimensionless hydrodynamic added mass coefficient

N_c bearing capacity

ρ density

S_{max} maximum allowable displacement

s_u undrained soil shear strength

T loading event period

t time

V volume

v_f velocity of plate

v_x horizontal component of velocity

v_y vertical component of velocity

z position

TABLE CAPTIONS

Table 1. Summary of bearing capacity factors ($\boldsymbol{N_c}$) and added mass coefficients ($\boldsymbol{N_{AM,2D}}$) for a plane strain plate

Table 2. Summary of bearing capacity factors ($\boldsymbol{N_c}$) and added mass coefficients ($\boldsymbol{N_{AM,3D}}$) for an axisymmetric disc

Table 3. Summary of parameters used in the illustrative example

FIGURE CAPTIONS

Figure 1. Failure mechanism from upper bound theorem for a (a) rough and (b) smooth plates and their accompanying hodographs (c) and (d)

Figure 2. Variations in the contributions of shear strength and the added mass of the material, with respect to the dimensionless group $\frac{\boldsymbol{s_u}}{\boldsymbol{B\rho a}}$ for (a) plane strain plate and (b) circular disc

Figure 3: Forces acting on embedded plate anchor during impulse snatch load.

Figure 4: Anchor movements during impulse snatch load with and without added mass effects

Figure A1: Variation of the cylinder and spheroid work rate integral with changing aspect ratio, AR

1. INTRODUCTION

Offshore renewable energy facilities are extending to floating structures in deeper waters, where stronger wind resources can be harnessed (Catapult, 2018). Meanwhile, floating oil and gas facilities continue to be deployed. Embedded plate anchors are an efficient solution for floating facilities particularly in soft seabeds. Plate anchors can be installed many ways, including drag-embedment, free-fall, screwing or via a suction anchor (Randolph & Gourvenec 2011, Aubeny 2017, O'Loughlin et al. 2017).

The anchor capacity is typically calculated as a multiple of the soil shear strength with an additional term representing the overburden if the failure mechanism is shallow (Randolph & Gourvenec 2011, Aubeny 2017). However, under rapid loading, additional capacity is created from the mass of the soil surrounding the plate. This added mass term is well recognised in fluid mechanics (e.g. Lamb 1895, Morison et al 1950, Sarpkaya & Isaacson 1981), and is routinely considered in the dynamic motion of floating structures and mooring lines. However, it is ignored in conventional geotechnical capacity analysis.

This technical note documents a method to quantify the added mass of the soil surrounding a plate anchor and the resulting additional resistance. The added mass effect is derived for conventional geotechnical collapse mechanisms in cohesive soils and compared to solutions from classical fluid mechanics. The influence of the contribution from added mass is illustrated for typical input conditions. This study does not consider the additional effects on soil strength (s_u) relevant to dynamic loading, namely the influence of their rapid and cyclic nature on s_u. The cyclic nature may reduce s_u, but dynamic loads with higher loading rates may also raise s_u due to the effect of strain rate on strength (Randolph & Gourvenec, 2017; Lunne & Andersen, 2007; Koumoto & Houlsby, 2001; Mitchell, 1993, 1964).

The general approach used in this paper to find the added mass term can also be applied to other materials, where similar effects are evident (e.g. Athani, S & Rognon, 2019). It can also be applied to other shapes of foundation – such as piles and caissons – via the same method if the velocity fields mobilised in the soil failure mechanism are identified, for example, experimentally or from a 3D finite element analysis.

2. BACKGROUND

Geotechnical bearing capacity theory

In undrained soils, the upper bound theorem is used to define a kinematically-admissible collapse mechanism for an embedded plate. Rigid sliding blocks of soil flow around a plate moving at a

velocity (v_f) as shown in Figures 1a and b. A hodograph showing the relative velocities throughout the mechanism is shown in Figures 1c and d. The internal work dissipation rate on each sliding plane, including the triangular blocks within the shear fan, is the product of the shear forces and relative velocities on the plane. Equating the work input to the dissipation gives the capacity due to the soil strength:

$$F_{su} = N_c s_u B \tag{2.1}$$

where N_c is the bearing capacity factor, s_u is the soil shear strength and B is the plate width. Solving the work equation yields $N_c = 3\pi + 2$ (Meyerhof 1951, Rowe & Davis 1982, Martin & Randolph, 2001).

Under rapid loading, at soil failure, additional work is required to accelerate the soil mass within the mechanism according to Newton's 2nd Law. The acceleration varies throughout the mechanism and the net effect is an additional component of resistance $F_{AM} = m_{AM} a$ where a is the acceleration of the plate and m_{AM} is a representative 'added mass'. As described later, this term can also be derived from the collapse mechanism. The total resistance force (F) on the plate after F_{su} is exceeded is

$$F = F_{su} + F_{AM} \tag{2.2}$$

Hydrodynamic added mass theory

In hydrodynamics, fluid flow around an accelerating plate is a classical problem. The force (F_{AM}) due to acceleration of inviscid fluid surrounding an object is analysed via the work done from the unsteady reaction forces on a body (Lamb, 1895). For a rigid body moving with speed v_f, the fluid kinetic energy is defined as

$$E = \rho v_f^2 \int_V \tilde{\kappa}\, dV = \frac{1}{2} m_{AM} v_f^2 \tag{2.3}$$

where ρ is the density of the fluid, V is the volume of fluid influenced by the flow field, m_{AM} is the lumped added mass term, and $\tilde{\kappa}$ is the local kinetic energy of the flow defined per unit mass, scaled by the body velocity (v_f). For planar flow, this is

$$\tilde{\kappa} = \frac{1}{2}\left(\frac{v_x^2 + v_y^2}{v_f^2}\right) \tag{2.4}$$

The v_x and v_y terms are the horizontal and vertical component velocities throughout the flow field when the object moves at v_f. The added mass term can be isolated using Equations 2.3 and 2.4

$$m_{AM} = \rho \int_V \frac{v_x^2 + v_y^2}{{v_f}^2}\, dV \tag{2.5}$$

The added mass term is found by integrating the velocities over the flow field caused the accelerating body and solutions exist for various rigid bodies (Newman, 2018). Using the potential flow solutions for the velocity field, the forces to accelerate a plane strain thin plate, or strip, of width B or a thin circular plate of diameter B in the axisymmetric case, are, respectively:

$$F_{AM} = m_{AM}a = \frac{\pi}{4}\rho B^2 a \qquad (2.6a)$$

$$F_{AM} = m_{AM}a = \frac{1}{3}\rho B^3 a \qquad (2.6b)$$

It is useful to define the dimensionless hydrodynamic added mass coefficient as $N_{AM,2D} = \frac{m_{AM}}{\rho B^2}$ or $N_{AM,3D} = \frac{m_{AM}}{\rho B^3}$ for the 2D plane strain and 3D axisymmetric cases; i.e. $N_{AM,2D} = \frac{\pi}{4}$ and $N_{AM,3D} = \frac{1}{3}$ respectively.

3. ANALYTICAL SOLUTION FOR FAM

The same approach as used for fluid flow can be applied to the deformation field defined by the geotechnical upper bound collapse mechanism, so the total force (F) can be written as

$$F = N_c s_u B + N_{AM}\rho B^2 a \qquad (2.7)$$

The velocities and volume of the sliding blocks within the plane strain collapse mechanism are integrated according to Equation 2.5, for both symmetrical and one-sided Prandtl failure mechanisms (Figures 1a,b).

For the symmetrical mechanism, Zones A and C give equal added mass contributions. The area (A) of the triangles, their velocity terms and resulting added mass contributions, m_{AM} are

$$A_{A,C} = \frac{B^2}{4};\ \left(\frac{v_x^2+v_y^2}{v_f^2}\right)_{A,C} = 1\ ;\ m_{AM}^{A,C} = \frac{1}{4}\rho B^2 \qquad (3.1)$$

In the fan shear zone B, the added mass term from integrating the velocities and areas from θ= 0 to $\frac{3\pi}{2}$ is

$$m_{AM}^{B} = \int_0^{3\pi/2} \frac{1}{v_f^2}\left(\frac{\sqrt{2}}{2}v_f\right)^2 \left(\sin^2\left(\frac{\pi}{4}+\delta\theta\right)+\cos^2\left(\frac{\pi}{4}+\delta\theta\right)\right)\frac{1}{2}\left(\frac{\sqrt{2}}{2}B\right)^2 d\theta = \frac{3\pi}{16}\rho B^2 \qquad (3.2)$$

Therefore, the total added mass term from applying Equation 2.5 over the whole failure mechanism is

$$m_{AM} = \left(\frac{1}{2}+\frac{3\pi}{8}\right)\rho B^2 = 1.678\rho B^2 \qquad (3.3)$$

This result is doubled for the one-sided Prandtl mechanism as half of the soil mass is moving at double the speed. The area (A) of the triangles, their velocity terms and resulting added masses in zones A and C are

$$A_{A,C} = \frac{B^2}{4};\ \left(\frac{v_x^2+v_y^2}{v_f^2}\right)_{A,C} = \frac{0+\left(\sqrt{2}v_f\right)^2}{v_f^2} = 2\ ;\ m_{AM}^{A,C} = \frac{1}{2}\rho B^2 \quad (3.4)$$

The added mass term in the fan shear zone B is

$$m_{AM}^{B} = \int_0^{3\pi/2} \frac{1}{v_f^2}\left(\sqrt{2}v_f\right)^2 \left(\sin^2\left(\frac{\pi}{4}+\delta\theta\right)+\cos^2\left(\frac{\pi}{4}+\delta\theta\right)\right)\frac{1}{2}\left(\frac{\sqrt{2}}{2}B\right)^2 d\theta = \frac{3\pi}{4}\rho B^2 \quad (3.5)$$

Therefore the total added mass term is

$$m_{AM} = \left(1+\frac{3\pi}{4}\right)\rho B^2 = 3.36\rho B^2 \quad (3.6)$$

4. NUMERICAL VERIFICATION OF F_{AM}

To check Equations 3.3 and 3.6, and explore m_{AM} for a circular plate, numerical analyses of the collapse mechanism were used to create deformation fields to independently determine the added mass term according to Equation 2.5. The numerical analysis utilised OxLim, a developing research software that uses Finite Element Limit Analysis (FELA) to solve geotechnical lower and upper bound solutions (Makrodimopoulos & Martin 2006, 2007, 2008). Four cases were considered; rough and smooth plates, with plane strain (strip) and circular (disc) shapes. The soil had homogenous undrained shear strength and unit weight.

The resulting bearing capacity factors obtained with the Tresca failure criterion matched to within 0.1% the exact plasticity solutions (Martin & Randolph 2001). The added mass coefficients were found from Equation 2.5, by integrating the velocities and volume of each element over the flow field within the full soil domain. For the plane strain case m_{AM} was within 2% of the analytical solution for the symmetrical mechanism (Equations 3.1 to 3.3) (Table 4). The added mass coefficient for the circular plate was lower than the plane strain case by a factor of ~2. This reflects the more localised failure mechanism, so less mass is accelerated (

Table 5).

5. SUMMARY AND APPLICATIONS

Summary of bearing and added mass coefficients

Table 4 and

Table 5 summarise the bearing capacity factor (N_c) and added mass coefficients (N_{AM}) determined using fluid mechanics and geotechnical approaches. For the inviscid flow solution, an equivalent bearing capacity factor was determined by developing the work equation analytically (see Appendix).

N_{AM} from the geotechnical collapse mechanism is significantly larger than from the inviscid flow field because of the different flow mechanisms. In inviscid fluids, there is negligible shear resistance within the material and the flow field develops such that the added mass term is minimised. However, in soil, with shear resistance, the optimal flow field minimises the dissipation. The resulting mechanism is larger resulting in a higher added mass.

These failure mechanisms that are exact for inviscid flow and rigid plastic flow represent extremes of the soil response across the potential range of loading rates. The different contributions of the shear strength and added mass to the total resistance are shown in Figure 6 across the range of dimensionless group $\frac{s_u}{B\rho a}$, which represents the balance between strength and inertia forces.

When $\frac{s_u}{B\rho a}$ is high, the shear strength term dominates, with the soil weightless in the limit $\frac{s_u}{B\rho a} \rightarrow \infty$ so the uplift capacity approaches the rigid plastic solution. Conversely, at low $\frac{s_u}{B\rho a}$, the added mass term dominates and in the limit the soil is strengthless.

The combined resistance from the bearing capacity and added mass coefficients of the inviscid and rigid plastic solutions are consistent with this transition. At high $\frac{s_u}{B\rho a}$ the rigid plastic mechanism offers lower total resistance and therefore the optimal failure mechanism, whereas at low $\frac{s_u}{B\rho a}$ the inviscid flow solution is lower. The transition is at $\frac{s_u}{B\rho a} \sim 1$ for plane strain, and ~0.08 for axisymmetry. In practice, the optimal mechanism that is mobilised could involve a mixture of the rigid plastic and inviscid flow fields, which are superposable. The transition between rigid plastic, inviscid flow, or a mixture, is likely to be smooth, similar to experimental observations for steady flow around a cylinder in soft soil (Sahdi et al. 2014).

Illustrative example

This example shows the influence of added mass for a typical design event of a force impulse (F_{load}) representing a snatch loading from a wave. Snatch loads are caused by dynamic mooring effects and can have a period ~10 times shorter than the wave itself (e.g. Hann et al. 2015, Lind et al. 2016). In geotechnical design, failure of a plate anchor can be defined at a displacement (S_{max}) of 10% of the plate diameter.

The impulse, F_{load} is represented by (Figure 7):

$$F_{load} = F_{min} + (F_{max} - F_{min}) \left(\frac{\sin\left(\frac{t-\alpha}{T}\right)}{\frac{t-\alpha}{T}} \right) \quad (5.1)$$

where F_{min} represents a steady static component of the mooring load and F_{max} is the peak load, varying with time, t, offset by α , with T being the event period. When F_{load} exceeds F_{su} the plate moves and Newmark's β method is used to calculate the resulting response (Figure 8). Therefore, the response of the plate, when $F_{load} > F_{su}$, is defined by the following equation of motion:

$$\sum F = F_{load} - F_{su} - F_{AM} = m_{plate} a \quad (5.2)$$

where m_{plate} is the mass of the plate. In Figure 7, F_{AM}, is the extra resistance force from the acceleration of the soil mass involved in the failure mechanism during the impulse load. The anchoring system withstands a peak load that is ~1.5 times greater than the geotechnical static capacity, due to the added mass contribution, without exceeding the allowable displacement of S_{max}= 0.1B (Figure 8c). This example shows that the added mass contribution can significantly enhance the capacity available to resist dynamic loads, beyond the geotechnical capacity typically used in practice. It is possible that the added mass, which is overlooked in design, are partly responsible for mooring systems failures being primarily due to mooring lines breaking, rather than anchors pulling out (Ma et al. 2019).

A second dynamic response for the same impulse load is also shown in Figure 8, for a case in which the mass of the plate is considered, but not the added soil mass. In this case the plate displacement from the loading event is >5m, approximately 10 times more than when the soil added mass is included (Figure 8c). This is consistent with the added mass being 10 times greater than the mass of the plate itself. A buried plate is efficient in this respect compared to other foundation types such as a vertically-loaded pile, for which the failure mechanism mobilises much less added mass. A summary of the parameters and values used in this illustrative example is included in Table 6.

6. CONCLUDING REMARKS

This technical note has documented a simple method for determining the added mass resistance during dynamic loading events on embedded foundations, utilising conventional geotechnical collapse mechanisms. These solutions are a geotechnical counterpart to the established added mass solutions derived for fluid flow. The solutions provide the additional contribution to the geotechnical resistance from the mass of soil accelerated in the failure mechanism during dynamic loading. An illustrative example shows that this additional resistance can significantly enhance the foundation capacity during dynamic loading events such as snatch loads within a mooring system. This general approach is not limited to embedded plate foundations but applies to other foundations, including shallow foundations or piles that are dynamically loaded. It provides a basis to quantify a potentially large additional component of geotechnical resistance that is overlooked in conventional design.

7. ACKNOWLEDGEMENTS

The authors acknowledge support of from the EPSRC Offshore Renewable Energy Supergen hub (Grant EPSRC EP/S000747/1).

APPENDIX

To find an upper bound plasticity solution for a failure mechanism or flow field, the internal work rate, W_i^V as an object moves through a continuum field of volume V with a constant undrained strength s_u is

$$W_i^V = s_u \int_V \dot{\gamma}_{max}, \quad N_c = \frac{W_i^V}{AUs_u} \tag{A1}$$

Where N_c is the work factor scaled by the anchor frontal area A and normal velocity U, and $\dot{\gamma}_{max}$ is the maximum local strain rate defined in terms of principal components or eigenvalues, λ_i of the infinitesimal strain rate tensor D

$$D = \frac{1}{2}(\nabla u + \nabla u^T) \tag{A2}$$

where u is the continuum velocity. As D is real and symmetric, it has real eigenvalues which can be found analytically in terms of the tensor trace $tr(D) = \sum \lambda_i$ and determinant $\det(D) = \prod \lambda_i$. In particular, the maximum strain rate for the Tresca condition is given by $\dot{\gamma}_{max} = 2\max|\lambda| = 2\max(\lambda_1, -\lambda_3)$ where $\lambda_1 > \lambda_2 > \lambda_3$. For the Von Mises condition, $\dot{\gamma}_{max} = \sqrt{2\sum \lambda_i^2}$. Dissipation due to the relative velocity at the object surface is neglected, which corresponds to the smooth case in the geotechnical analysis.

Incompressible Irrotational 2D and Axisymmetric Flow

If the velocity field is irrotational, it can be defined by a potential function $u = \nabla\phi$ meaning $D = H\phi$, where H is the Hessian matrix. If the flow is also incompressible then $\nabla \cdot u = 0$ and the potential satisfies the Laplace equation $\nabla^2\phi = tr(D) = 0$. Classical solutions for many flow potentials are known, such as from Lamb (1895), however the Hessian of a potential and its eigenvalues have not been well studied. If a 3D flow defined in coordinates q_1, q_2, q_3 is 2D or axisymmetric about the coordinate q_3 then $\frac{\partial\phi}{\partial q_3} = 0$ and the strain rate matrix takes the general form

$$D = H(\phi) = \begin{bmatrix} D_{11} & D_{12} & 0 \\ D_{12} & D_{22} & 0 \\ 0 & 0 & D_{33} \end{bmatrix} \tag{A3}$$

where $D_{33} = -D_{11} - D_{22}$ due to incompressibility. Since the q_3 rows and columns are linearly independent there is a trivial mean eigenvalue $\lambda_2 = D_{33} = -D_{11} - D_{22}$. With that eigenvalue known, the characteristic equation is reduced to a quadratic and the other eigenvalues are

$$\lambda_{1,3} = \frac{1}{2}\left[-\lambda_2 \pm \sqrt{\lambda_2^2 - 4\det(D_{2d})}\right] \tag{A4}$$

Where $\det(D_{2d}) = D_{11}D_{22} - D_{12}^2$. Substitution gives the axisymmetric maximum strain rate for the two failure criteria as

$$\dot{\gamma}_{max} = \begin{cases} |\lambda_2| + \sqrt{\lambda_2^2 - 4\det(D_{2d})}, & Tresca \\ 2\sqrt{\lambda_2^2 - \det(D_{2d})}, & Von\ Mises \end{cases} \tag{A5}$$

For fully 2D flow we must also have $D_{33} = \lambda_2 = 0$ and so $\dot{\gamma}_{max} = 2\sqrt{-\det(D_{2d})}$ for either failure criterion.

2D Flows Using Complex Variables

For 2D potential flow with a holomorphic complex potential $\Phi(\zeta)$, where $\zeta = x + iy = re^{i\theta}$, $\frac{d\Phi}{d\zeta} = \frac{d\Phi}{dx} = \frac{d\Phi}{d(iy)}$. This means the strain rate tensor and maximum strain rate are

$$D_{xx} = -D_{yy} = Re|\Phi''|,\ D_{xy} = -Im|\Phi''|,\ \dot{\gamma}_{max} = 2|\Phi''| \tag{A6}$$

Complex variables make it simple to map any potential Φ to a new coordinate system using a transformation function $\chi = f(\zeta)$. Using the chain rule, the complex velocity is

$$w = u_x - iu_y = \frac{d\Phi}{d\chi} = \frac{\Phi'}{\chi'} \tag{A7}$$

Where $\chi' = \frac{d\chi}{d\zeta}$. Applying the product and chain rule again to give the second derivative and strain rate as

$$\frac{d^2\Phi}{d\chi^2} = \frac{d}{d\chi}\left(\frac{\Phi'}{\chi'}\right) = \frac{\Phi'' - \Phi'\chi''/\chi'}{\chi'^2} \rightarrow \dot{\gamma}_{max} = \frac{2}{J}\left|\Phi'' - \Phi'\frac{\chi''}{\chi'}\right| \tag{A8}$$

Where $J = \left|\frac{d\chi}{d\zeta}\right|^2$ is the Jacobian. The volume integral over V will also be adjusted in the transformed space as $dV = d\xi d\varphi = Jdxdy$. Therefore, the Jacobians cancel and the work per unit depth is

$$W_i^v = s_u \int_V 2\left|\Phi'' - \Phi'\frac{\chi''}{\chi'}\right| dxdy \tag{A9}$$

General elliptical cylinder

The circle defined by $\zeta = ae^{i\theta}$ is mapped to an ellipse using the transformation $\chi = \zeta - \epsilon a^2\zeta^{-1}$. The area (per unit length) of the resulting ellipse is $A = 2a(1+\epsilon)$ and the aspect ratio is $AR = \frac{1-\epsilon}{1+\epsilon}$, so setting $\epsilon = 0$ recovers a circle and $\epsilon = 1$ results in a flat plate. Lamb (1895) shows a dipole $\Phi =$

$k\zeta^{-1}$ describes the flow induced by this moving ellipse, where k is the dipole strength. Computing $\Phi' = -k\zeta^{-2}$ and $\chi' = 1 + \epsilon a^2\zeta^{-2}$, the complex velocity is

$$w = -\frac{k\zeta^{-2}}{1+\epsilon a^2\zeta^{-2}} \tag{A10}$$

Therefore, $k = Ua^2(1+\epsilon)$ to achieve surface velocity $w = -U$ when $r = a, \theta = 0, \pi$. Note the velocity is singular at $\epsilon = 1, r = a, \theta = \pm\frac{\pi}{2}$, corresponding to the corners of a flat plate. Computing $\Phi'' = 2k\zeta^{-3}$ and $\chi'' = -2\epsilon a^2\zeta^{-3}$ and substituting gives the second derivative as

$$\frac{d^2\Phi}{d\chi^2} = \frac{2k\zeta^{-3}}{(1+\epsilon a^2\zeta^{-2})^3} \tag{A11}$$

From which the components of D and $\dot{\gamma}_{max}$ are determined. Finally, the work rate for a general elliptical cylinder is then

$$W_i^v = 2s_u \int_0^{2\pi}\int_a^{\infty} \left|\frac{2k\zeta^{-3}}{(1+\epsilon a^2\zeta^{-2})^3}\right| rdrd\theta = 16ks_u \int_0^{\frac{\pi}{2}}\int_a^{\infty} \frac{drd\theta}{|r^2+\epsilon a^2 e^{-2i\theta}|} \tag{A12}$$

Which gives $N_c = 4\pi$ for a circle ($\epsilon = 0$) and $N_c \approx 13.75$ for the plate. The full range of integration can be determined numerically and the result is summarised in Figure A1.

Sphere

In axisymmetric flow, we cannot use the complex variable coordinate system, but choosing coordinates aligned with the body geometry ensures $\phi = Q_1(q_1)Q_2(q_2)$. For example, the flow induced by a sphere is described by the potential $\phi = \frac{1}{2}Ua^3r^{-2}\cos\theta = R(r)\Theta(\theta)$. Note the axisymmtric variable $q_3 = \varphi$ does not appear. The strain tensor components are more complex due to the metrics not being constant, and are given by

$$D_{rr} = R''\Theta = 2\beta\cos\theta$$

$$D_{\theta\theta} = \frac{R'}{r}\Theta + \frac{R}{r^2}\Theta'' = -\beta\cos\theta$$

$$D_{r\theta} = \left[\frac{R'}{r} - \frac{R}{r^2}\right]\Theta = \beta\sin\theta \tag{A13}$$

Where $\beta = \frac{3Ua^3}{2r^4}$. As such, we have $\lambda_2 = -\beta\cos\theta$ and $\det(D_{2D}) = -\beta^2(2\cos^2\theta + \sin^2\theta)$ and so

$$\frac{\dot{\gamma}_{max}}{\beta} = \begin{cases} |\cos\theta| + \sqrt{5\cos^2\theta + 4}, & Tresca \\ 2\sqrt{2\cos^2\theta + 1}, & Von\ Mises \end{cases} \tag{A14}$$

Integration gives the work integral as

$$W_i^V = 2\pi \int_0^{\pi} \int_0^{\infty} \dot{\gamma}_{max}\, r^2 \sin\theta \; dr \; d\theta \rightarrow \frac{W_i^V}{AUs_u} = 3\int_0^{\pi} \frac{\dot{\gamma}_{max}}{\beta} sin\theta \; d\theta \approx \begin{cases} 17.165, & Tresca \\ 15.255, & Von\ Mises \end{cases}$$

(A15)

where $A = \pi a^2$ is the frontal area.

Oblate Spheroid Coordinates

Obtaining solutions for more general sphere-like shapes requires a more cumbersome coordinate system such as oblate spheriodal coordinates ζ, μ, φ defined as

$$x = a\mu\zeta,\ y = \rho\cos\varphi,\ z = \rho\sin\varphi,\ \rho^2 = a^2(1-\mu^2)(1+\zeta^2) \quad \text{(A16)}$$

where $0 \le \zeta < \infty$, $-1 \le \mu \le 1$ and a is the focal radius.

The scale factors and Jacobian are

$$h_\zeta = a\sqrt{\frac{\zeta^2+\mu^2}{1+\zeta^2}},\ h_\mu = a\sqrt{\frac{\zeta^2+\mu^2}{1-\mu^2}},\ h_\varphi = \rho,\ J = a^3(\zeta^2+\mu^2) \quad \text{(A17)}$$

Finally, the independent components of the strain matrix applied to an axisymmetric field $\phi = Z(\zeta)M(\mu)$ are

$$D_{\zeta\zeta} = \frac{M}{h_\zeta}\frac{\partial}{\partial\zeta}\frac{Z'}{h_\zeta} + \frac{ZM'}{h_\zeta h_\mu^2}\frac{\partial h_\zeta}{\partial\mu} = \frac{Z''M}{h_\zeta^2} + \frac{\mu ZM' - \zeta Z'M}{h_\mu^2(\zeta^2+\mu^2)}$$

$$D_{\mu\mu} = \frac{Z}{h_\mu}\frac{\partial}{\partial\mu}\frac{M'}{h_\mu} + \frac{Z'M}{h_\mu h_\zeta^2}\frac{\partial h_\mu}{\partial\zeta} = \frac{ZM''}{h_\mu^2} + \frac{\zeta Z'M - \mu ZM'}{h_\zeta^2(\zeta^2+\mu^2)}$$

$$D_{\zeta\mu} = \frac{h_\mu M'}{2h_\zeta}\frac{\partial}{\partial\zeta}\frac{Z}{h_\mu^2} + \frac{h_\zeta Z'}{2h_\mu}\frac{\partial}{\partial\mu}\frac{M}{h_\zeta^2} = \frac{Z'M'}{h_\zeta h_\mu} - \frac{\zeta ZM' + \mu Z'M}{h_\zeta h_\mu(\zeta^2+\mu^2)} \quad \text{(A18)}$$

3D Disc

A disc of radius a is obtained on $\zeta = 0$ and the flow potential induced by perpendicular motion of this disc is given by $= \frac{2Ua}{\pi}\mu(1 - \zeta\cot^{-1}\zeta)$ (Lamb 1895). Therefore

$$Z = 1 - \zeta\cot^1\zeta,\ Z' = \frac{\zeta}{1+\zeta^2} - \cot^1\zeta,\ Z'' = \frac{2}{(1+\zeta^2)^2}$$

$$M = \frac{2Ua}{\pi}\mu,\ M' = \frac{2Ua}{\pi},\ M'' = 0 \quad \text{(A19)}$$

Substituting these into the oblate strain matrix formula and integrating over the oblate coordinates gives

$$\frac{W_i^V}{\pi a^2 Us_u} \approx \begin{cases} 16.198, & Tresca \\ 14.842, & Von\ Mises \end{cases} \quad \text{(A20)}$$

Which are quite similar to the sphere results. Figure A1 shows the value of scaled work as a function of the oblate spheroid aspect ratio (adjusted by using different ζ surfaces). The work is fairly constant, but is at a minimum for spheroids around $AR \sim 0.15$

8. REFERENCES

Athani, S., & Rognon, P. (2019). Inertial drag in granular media. Physical Review Fluids, 4(12), 124302.Aubeny, C., (2017). Geomechanics of Marine Anchors. CRC Press.

ORE Catapult, (2018). Report: Macroeconomic benefits of floating offshore wind in the UK. Report for the Crown Estate Scotland.

Einav, I. and Randolph, M.F., (2005). Combining upper bound and strain path methods for evaluating penetration resistance. International journal for numerical methods in engineering, 63(14), pp.1991-2016.

Hann, M., Greaves, D. and Raby, A., (2015). Snatch loading of a single taut moored floating wave energy converter due to focussed wave groups. Ocean Engineering, 96, pp.258-271.

Koumoto, T. and Houlsby, G. T. (2001). Theory and practice of the fall cone test. Geotechnique, 51(8):701–712

Lamb, H., (1895). Hydrodynamics. Cambridge University Press.

Lind, S.J., Stansby, P.K. and Rogers, B.D., (2016). Fixed and moored bodies in steep and breaking waves using SPH with the Froude–Krylov approximation. Journal of Ocean Engineering and Marine Energy, 2(3), pp.331-354.

Lunne, T., & Andersen, K. H. (2007). Soft clay shear strength parameters for deepwater geotechnical design. In Offshore Site Investigation and Geotechnics: Confronting New Challenges and Sharing Knowledge. Society of Underwater Technology.

Ma K.T., Luo Y., Kwan, T. & Wu, Y. (2019). Mooring system reliability. Chapter 13 in Mooring System Engineering for Offshore Structures, Gulf Professional Publishing. 255-279.

Makrodimopoulos, A. & Martin, C.M. (2006). Lower bound limit analysis of cohesive-frictional materials using second-order cone programming. International Journal for Numerical Methods in Engineering, Vol. 66, No. 4, pp 604-634.

Makrodimopoulos, A. & Martin, C.M. (2007). Upper bound limit analysis using simplex strain elements and second-order cone programming. International Journal for Numerical and Analytical Methods in Geomechanics, Vol. 31, No. 6, pp 835-865.

Makrodimopoulos, A. & Martin, C.M. (2008). Upper bound limit analysis using discontinuous quadratic displacement fields. Communications in Numerical Methods in Engineering, Vol. 24, No. 11, pp 911-927.

Meyerhof, G.G., (1951). The ultimate bearing capacity of foundations. Geotechnique, 2(4), pp.301-332.

Mitchell, J. K. (1993). Fundamentals of soil behaviour (2nd edition). John Wiley and Sons, New York

Mitchell, J. K. (1964). Shearing resistance of soils as a rate process. Journal of the Soil Mechanics and Foundations Division, ASCE, 90(SM 1):29–61

Morison, J. R.; O'Brien, M. P.; Johnson, J. W.; Schaaf, S. A. (1950), The force exerted by surface waves on piles, Petroleum Transactions, American Institute of Mining Engineers, 189: 149–154, doi:10.2118/950149-G

Newman, J.N., (2018). Marine hydrodynamics. MIT press.

O'Loughlin, C.D., White, D.J. and Stanier, S.A., (2017). Plate Anchors for Mooring Floating Facilities–A View Towards Unlocking Cost and Risk Benefits. In Offshore Site Investigation Geotechnics 8th International Conference Proceeding (Vol. 978, No. 986, pp. 978-986). Society for Underwater Technology.

Randolph, M. and Gourvenec, S., (2017). Offshore geotechnical engineering. CRC press.

Rowe, R. K., & Davis, E. H. (1982). The behaviour of anchor plates in clay. Geotechnique, 32(1), 9-23.

Sahdi F., Gaudin C., White D.J. Boylan, N.P. & Randolph M.F. (2014). Centrifuge modelling of active slide-pipeline loading in soft clay Géotechnique, 64(1):16-27

Sarpkaya, T.; Isaacson, M. (1981), Mechanics of wave forces on offshore structures, New York: Van Nostrand Reinhold, ISBN 0-442-25402-4

TABLES

Table 4. Summary of bearing capacity factors (N_c) and added mass coefficients ($N_{AM,2D}$) for a plane strain plate

Method	N_c	$N_{AM,2D}$
Fluid inviscid flow field	13.750	0.79
Geotechnical analytical UB[#]	11.425	1.678[c], 3.356[d]
Geotechnical numerical UB (OxLim)	11.439[a], 11.431[b]	1.648

[#]Meyerhof (1951)

[a, b] Rough and smooth analyses

[c, d] Prandtl one and two-way mechanisms

Table 5. Summary of bearing capacity factors (N_c) and added mass coefficients ($N_{AM,3D}$) for an axisymmetric disc

Method	N_c	$N_{AM,3D}$
Fluid inviscid flow field	16.198[e], 14.842[f]	0.33
Geotechnical analytical UB[#]	13.11[a], 12.42[b]	-
Geotechnical numerical UB (OxLim)	13.13[a], 12.435[b]	0.548[a], 0.599[b]

[#]Martin & Randolph (2001)

[a, b] Rough and smooth analyses

[e, f] Tresca, Von Mises

443 Table 6. Summary of parameters used in the illustrative example

Input Parameters	Value	Units
Plate properties		
Plate diameter, B	5	m
Soil Properties		
Soil density, ρ	1800	kg/m^3
Undrained shear strength s_u	20	kPa
Geotechnical capacity		
Bearing factor, N_c	13.11	-
Geotechnical capacity F_{su}	5128.65	kN
Added mass resistance		
Added mass coefficient N_{AM}	0.548	-
Added mass	123,300	kg

444

FIGURES

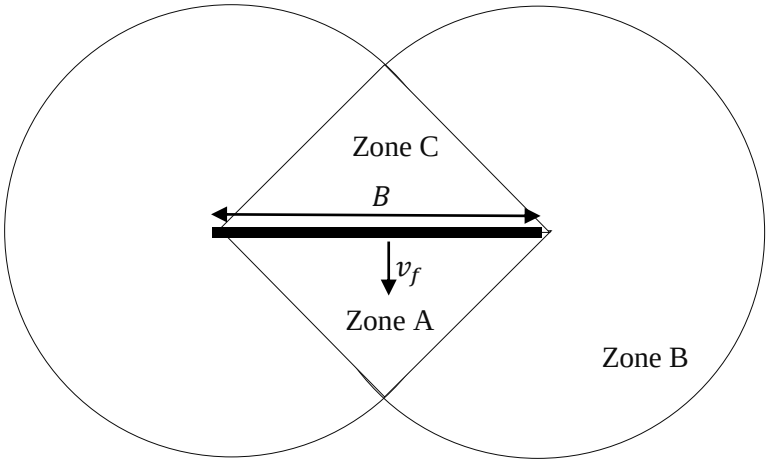

(a)

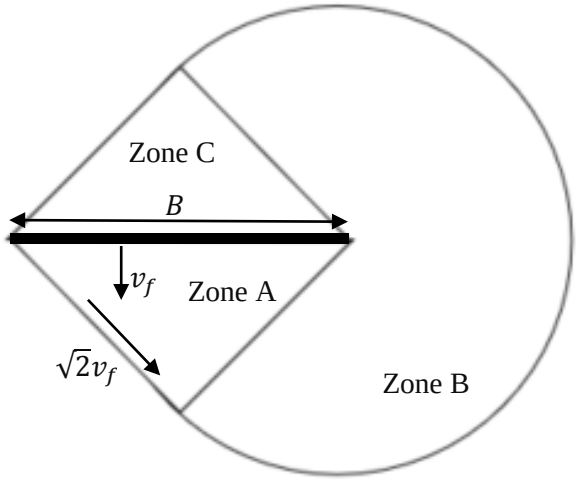

(b)

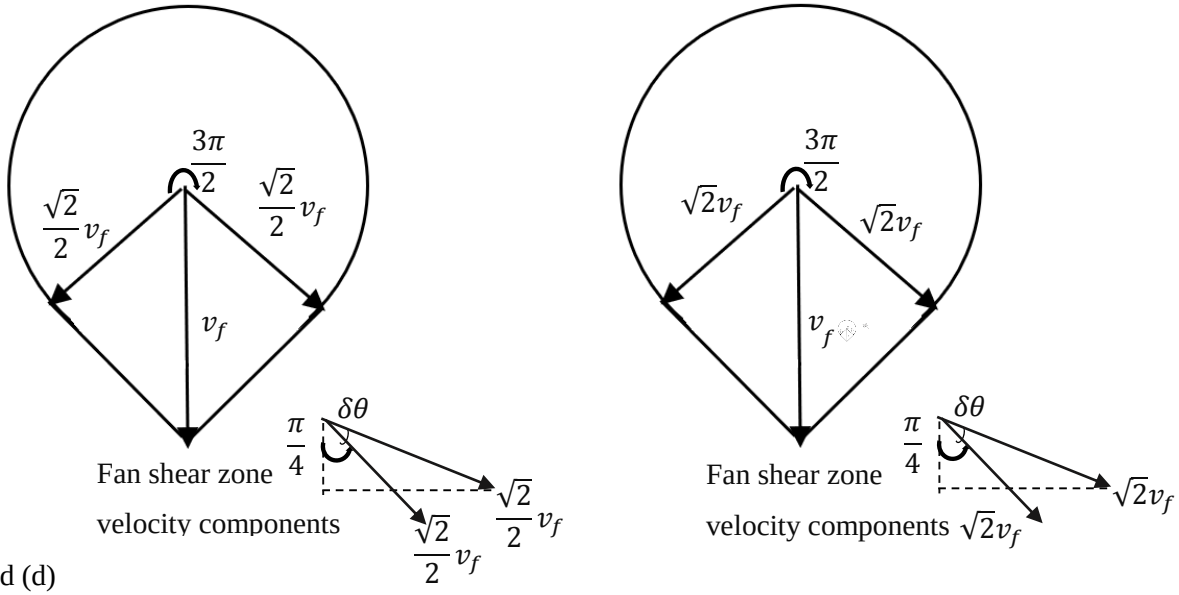

(c) and (d)

Figure 5. Failure mechanism from upper bound theorem for a (a) rough and (b) smooth plates and their accompanying hodographs (c) and (d)

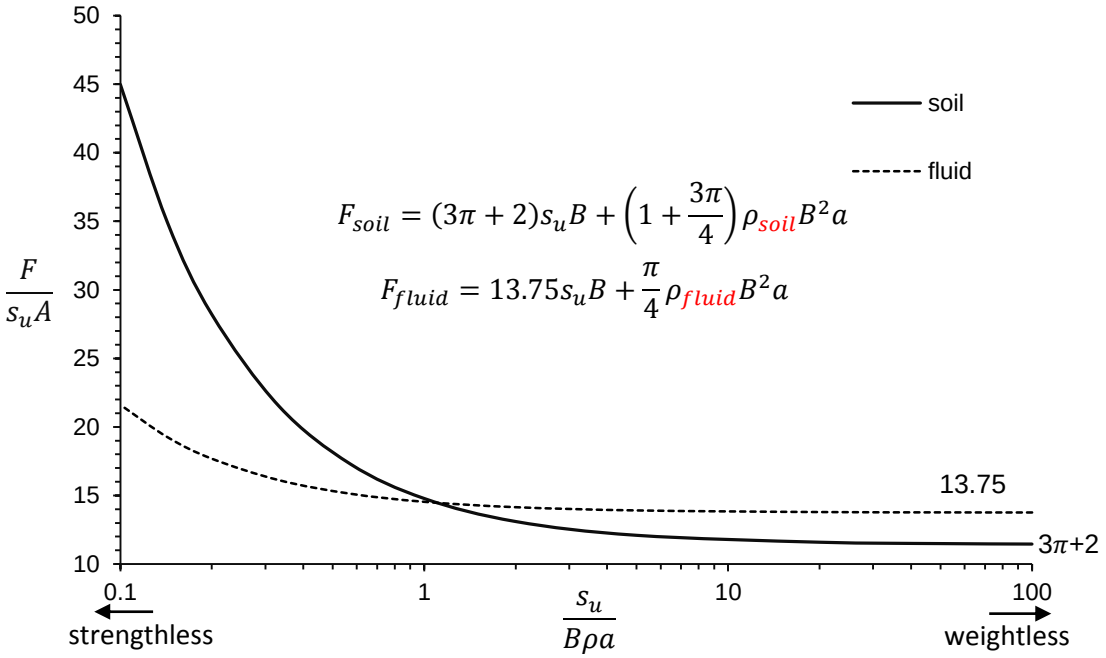

(a)

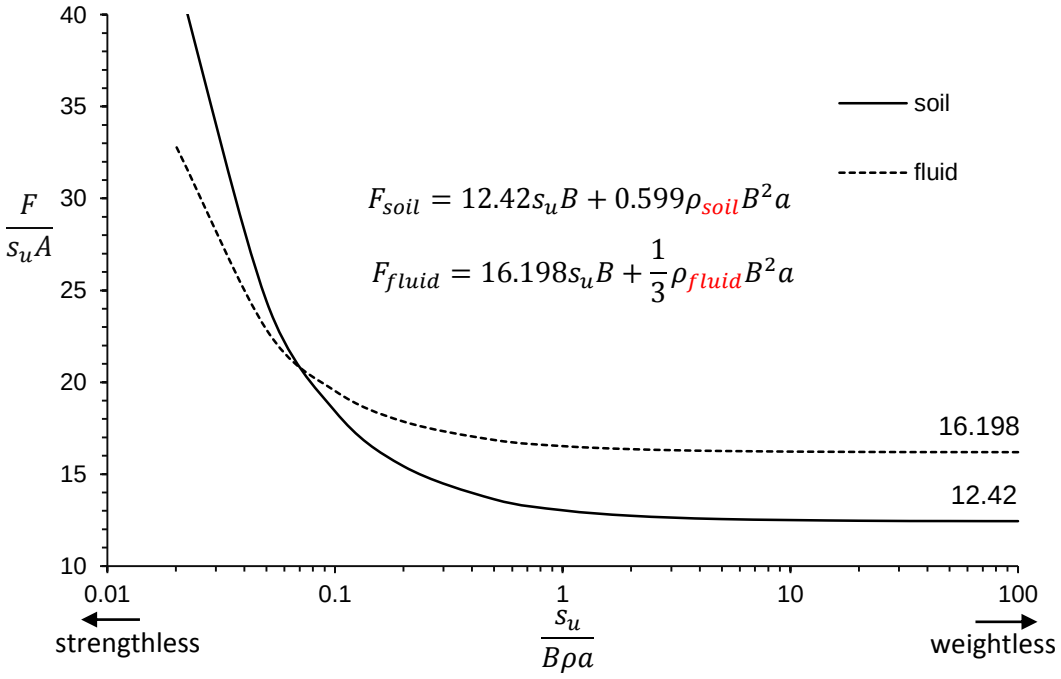

(b)

Figure 6. Variations in the contributions of shear strength and the added mass of the material, with respect to the dimensionless group $\frac{s_u}{B\rho a}$ for (a) plane strain plate and (b) circular disc

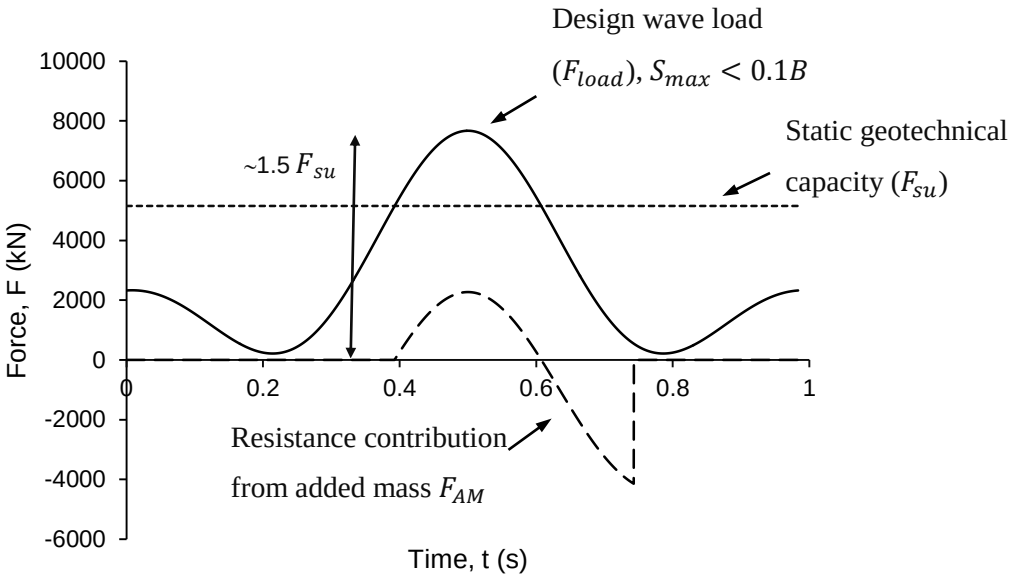

Figure 7: Forces acting on embedded plate anchor during impulse snatch load.

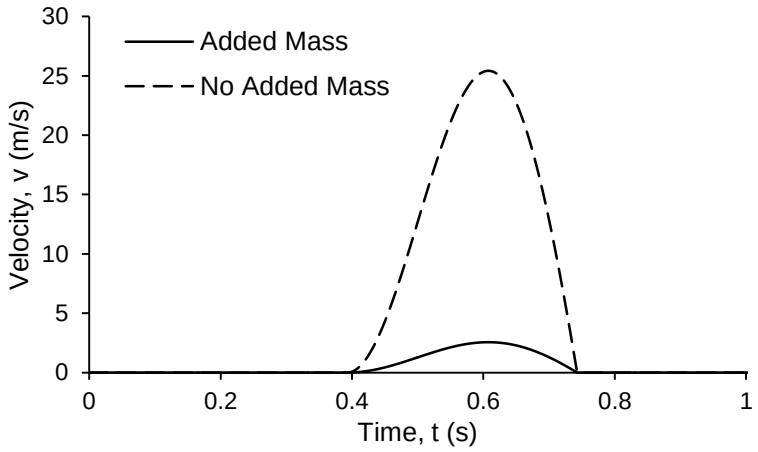

a

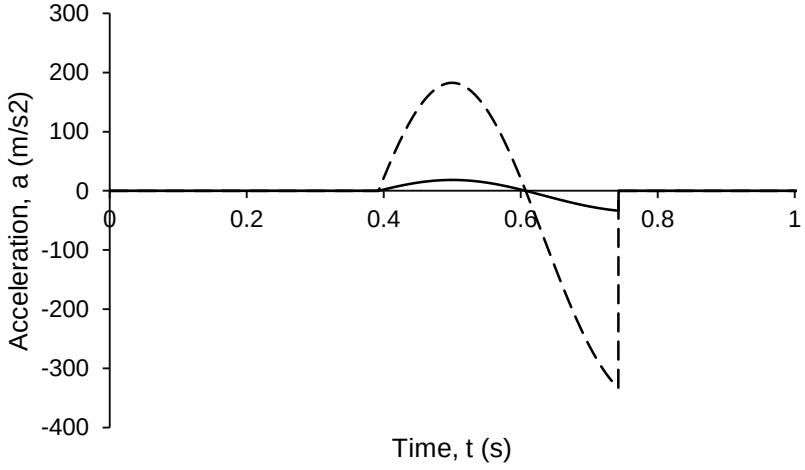

b

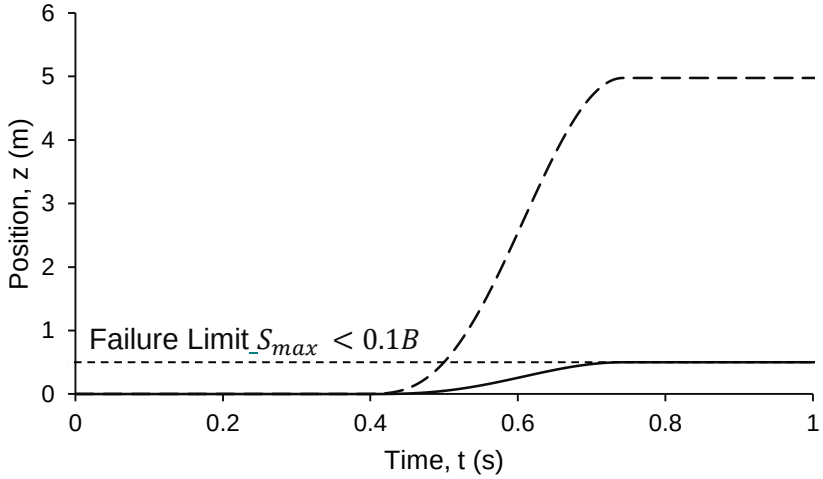

c

Figure 8: Anchor movements during impulse snatch load with and without added mass effects

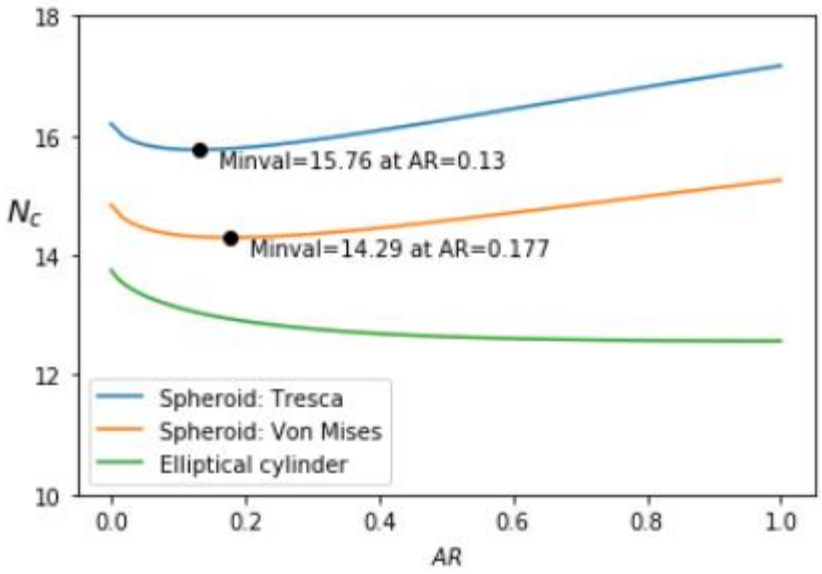

Figure A1: Variation of the cylinder and spheroid work rate integral with changing aspect ratio, AR

TABLES

Table 1. Summary of bearing capacity factors (N_c) and added mass coefficients ($N_{AM,2D}$) for a plane strain plate

Method	N_c	$N_{AM,2D}$
Fluid inviscid flow field	13.750	0.79
Geotechnical analytical UB[#]	11.425	1.678[c], 3.356[d]
Geotechnical numerical UB (OxLim)	11.439[a], 11.431[b]	1.648

[#]Meyerhof (1951)

[a, b] Rough and smooth analyses

[c, d] Prandtl one and two-way mechanisms

Table 2. Summary of bearing capacity factors (N_c) and added mass coefficients ($N_{AM,3D}$) for an axisymmetric disc

Method	N_c	$N_{AM,3D}$
Fluid inviscid flow field	16.198[e], 14.842[f]	0.33
Geotechnical analytical UB[#]	13.11[a], 12.42[b]	-
Geotechnical numerical UB (OxLim)	13.13[a], 12.435[b]	0.548[a], 0.599[b]

[#]Martin & Randolph (2001)

[a, b] Rough and smooth analyses

[e, f] Tresca, Von Mises

Table 3. Summary of parameters used in the illustrative example

Input Parameters	Value	Units
Plate properties		
Plate diameter, B	5	m
Soil Properties		
Soil density, ρ	1800	kg/m^3
Undrained shear strength s_u	20	kPa
Geotechnical capacity		
Bearing factor, N_c	13.11	-
Geotechnical capacity F_{su}	5128.65	kN
Added mass resistance		
Added mass coefficient N_{AM}	0.548	-
Added mass	123,300	kg

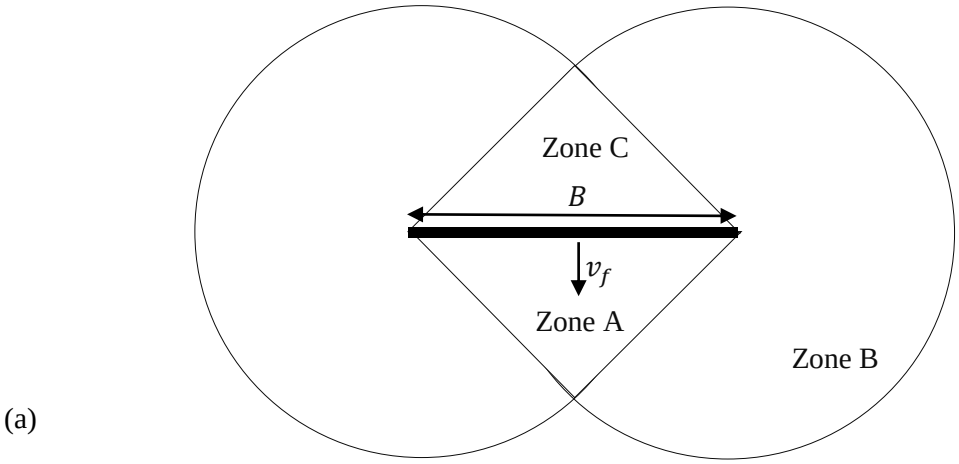

(a)

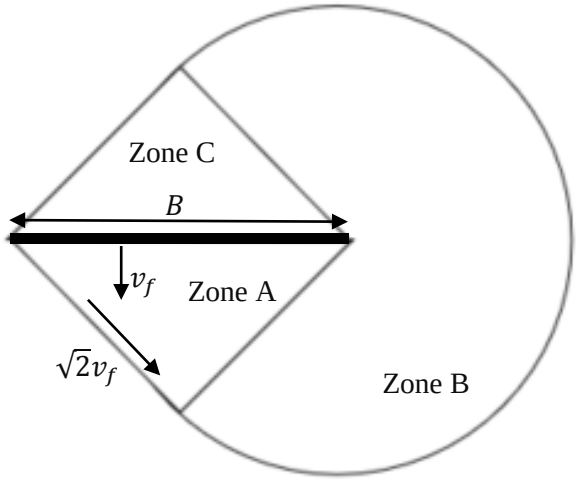

(b)

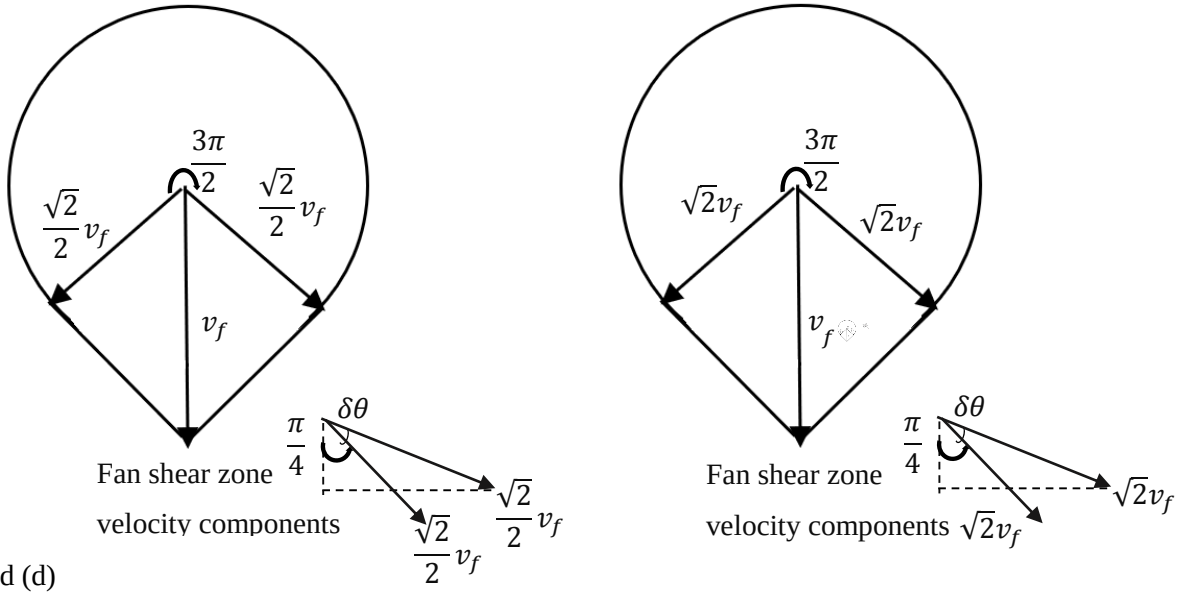

(c) and (d)

Figure 1. Failure mechanism from upper bound theorem for a (a) rough and (b) smooth plates and their accompanying hodographs (c) and (d)

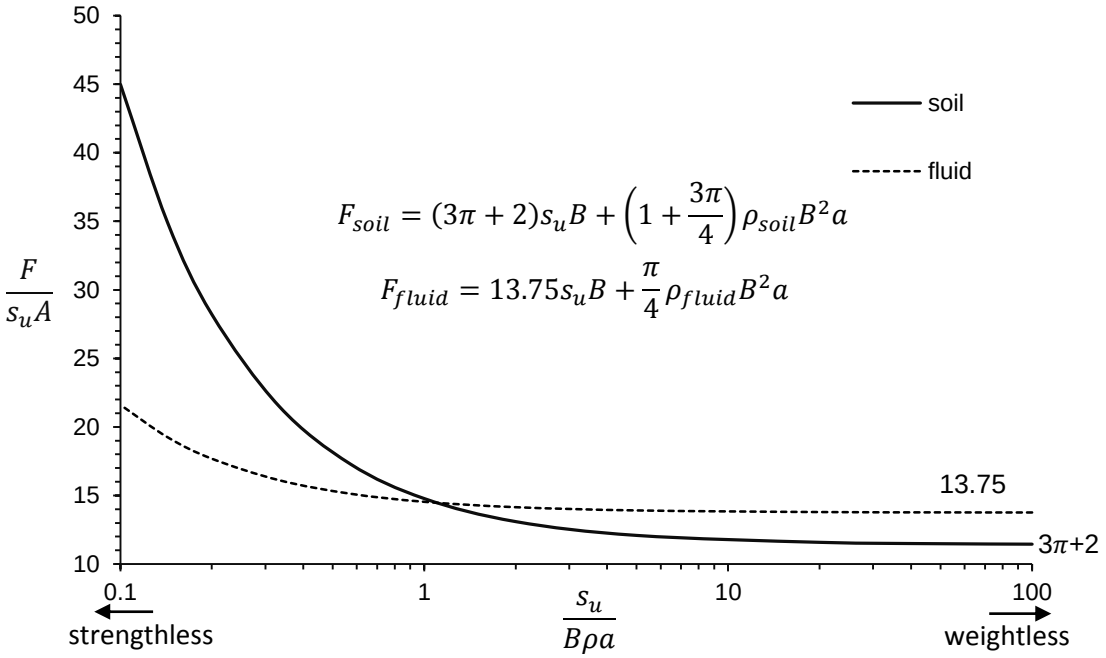

(a)

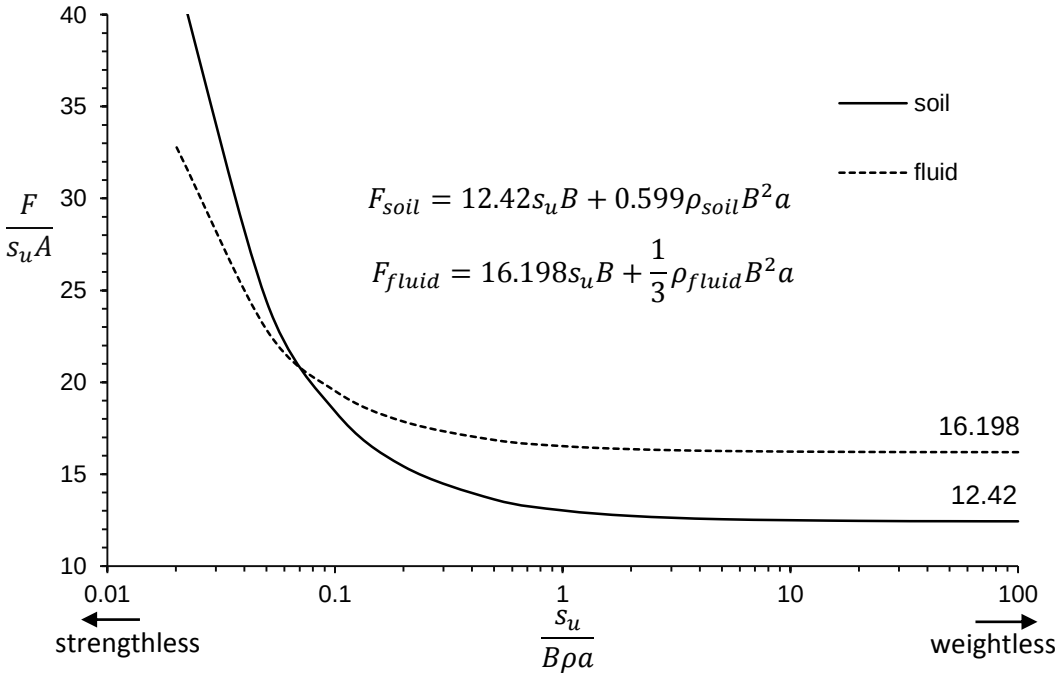

(b)

Figure 1. Variations in the contributions of shear strength and the added mass of the material, with respect to the dimensionless group $\frac{s_u}{B\rho a}$ for (a) plane strain plate and (b) circular disc

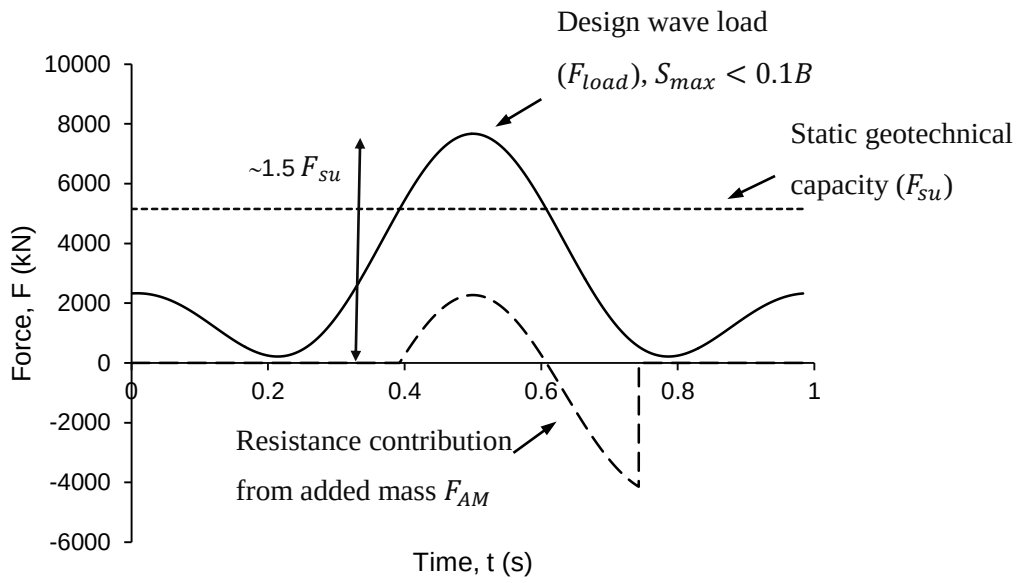

Figure 1: Forces acting on embedded plate anchor during impulse snatch load.

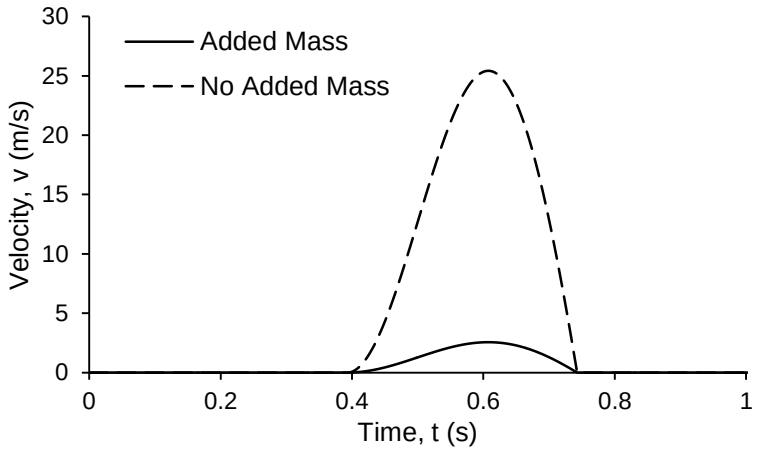

a

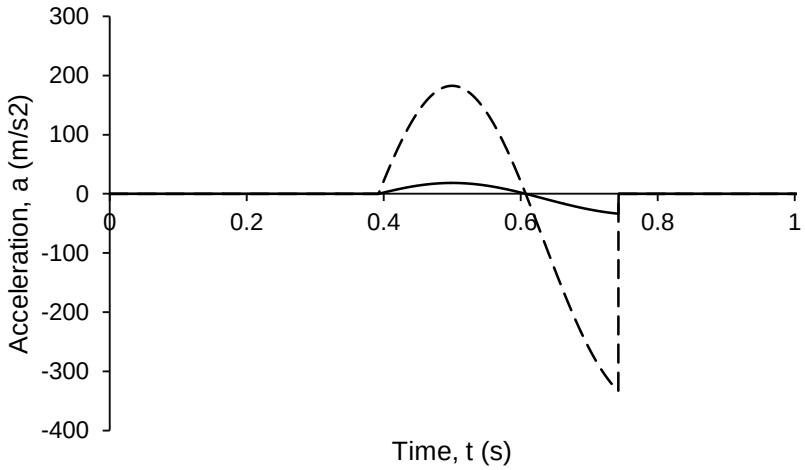

b

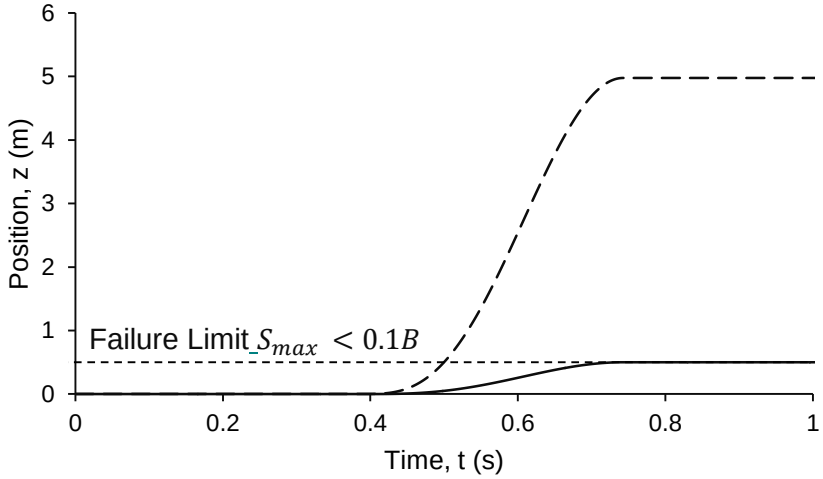

c

Figure 1: Anchor movements during impulse snatch load with and without added mass effects

Figure

Click here to access/download;Figure;figureA1.jpg